


## Article

# A Research on Rotor/Ship Wake Characteristics under Atmospheric Boundary Layer Conditions

Guoqiang Li <sup>1,2</sup>, Qing Wang <sup>3,\*</sup> , Qijun Zhao <sup>4</sup>, Guoqing Zhao <sup>4</sup>, Fei Feng <sup>5</sup> and Linxin Wu <sup>2</sup>

<sup>1</sup> College of Aerospace Science and Engineering, National University of Defense Technology, Changsha 410073, China; cardcl@126.com

<sup>2</sup> Low Speed Aerodynamics Institute, China Aerodynamics Research and Development Center, Mianyang 621000, China; 18810786853@163.com

<sup>3</sup> School of Energy and Power Engineering, Lanzhou University of Technology, Lanzhou 730050, China

<sup>4</sup> College of Aerospace Engineering, Nanjing University of Aeronautics and Astronautics, Nanjing 210016, China; zhaoqijun@nuaa.edu.cn (Q.Z.); zhaoguoqing@nuaa.edu.cn (G.Z.)

<sup>5</sup> China Academy of Launch Vehicle Technology, Beijing 100076, China; ff@foxmail.com

\* Correspondence: wangqing\_lut@foxmail.com

**Abstract:** The environment for the shipboard landing and takeoff of helicopters is extremely complex and significantly affects their safe flight. To address the intricate characteristics of the flow field during these operations, a simulation method suitable for rotor/ship wake vortex interaction is developed. This method couples the Delayed Detached Eddy Simulation (DDES) method and the momentum source method. The simulation of flow field characteristics of the SFS2 ship model under different conditions reveals that, in a rotor/ship coupling scenario, the inflow velocity in the wake zone of the flight deck is distributed in a “W” shape due to the influence of the rotor blade tip vortex. Under wind shear conditions, the rotor’s influence on the wake is reduced, resulting in smaller velocity fluctuations compared to uniform inflow conditions. Moreover, the detached eddy is suppressed to some extent. It can be concluded that shear flow mitigates the unsteady characteristics of the ship’s wake zone to some extent, which is beneficial to helicopter operations during takeoff and landing.

**Keywords:** rotor; wake; CFD; helicopter



**Citation:** Li, G.; Wang, Q.; Zhao, Q.; Zhao, G.; Feng, F.; Wu, L. A Research on Rotor/Ship Wake Characteristics under Atmospheric Boundary Layer Conditions. *Aerospace* **2023**, *10*, 816. <https://doi.org/10.3390/aerospace10090816>

Academic Editor: Anthony D. Gardner

Received: 26 July 2023

Revised: 25 August 2023

Accepted: 28 August 2023

Published: 18 September 2023



**Copyright:** © 2023 by the authors. Licensee MDPI, Basel, Switzerland. This article is an open access article distributed under the terms and conditions of the Creative Commons Attribution (CC BY) license (<https://creativecommons.org/licenses/by/4.0/>).

## 1. Introduction

The unique operation conditions of ship-based helicopters are significantly different from the landing environment of land-based ones. Particularly, the landing on small and medium-sized ships involves more maneuvers and greater difficulty than landing on land [1]. The presence of irregular waves significantly affects the pitch, roll, heave and other motions of ships, resulting in the irregular movement of the helicopter flight deck. The irregular sea wind motions, coupled with the helicopter inflow conditions, affects the rotor’s aerodynamic characteristics. The wake characteristics of ship structures, such as vortex, turbulence and inflow velocity variations, also influence rotor aerodynamics. Overall, the extremely complex landing and takeoff environment of ship-based helicopters seriously affects their safe flight. Consequently, researchers in both the domestic and international arenas have conducted theoretical, numerical simulation and experimental studies to investigate the landing characteristics of ship-based helicopters. Numerous landing flight envelopes of ship-based helicopters have been developed to enhance the safety of helicopter landings and takeoffs.

Extensive theoretical and experimental studies have been conducted both at home and abroad on the airwake flow field in various ship environments to analyze the turbulent flow field during ship-based helicopter landings. Gu and Ming [2] employed a seven-hole probe to investigate the flow field characteristics of the aft flight deck of a destroyer during

actual navigation, providing the test basis for developing the Wind-Over-Deck (WOD) envelope to ensure safe helicopter takeoffs and landings. Polsky and Bruner [3,4] performed time-accurate computational simulations of the unsteady flow field structure of the wake of an LHA model and compared them with test results. Bunnell [5] numerically simulated the varying rotor loads during shipboard landings of UH-60 helicopters and analyzed the influence of inflow, turbulence and other factors on the varying rotor loads. Reddy, Toffoletto and Jones [6] performed numerical simulation of the flow field of the simple frigate shape (SFS) model and investigated the velocity field characteristics of the ship's wake field. Rajagopalan, Schaller and Wadcock [7] employed Particle Image Velocimetry (PIV) [8,9] in wind tunnel tests to investigate the flow field characteristics of the V-22 Osprey during takeoff and landing on a helicopter carrier and compared them with CFD simulation results to verify their agreement. Sezerzol, Sharma and Long [10] simulated the flow field characteristics of LHA and LPD-17 models using the CFD method, demonstrating significant flow field velocity fluctuations with obvious unsteady characteristics. Zhao [11,12] employed PIV in wind tunnel tests to investigate the flow field characteristics of the ship wake, revealing that selecting an appropriate helicopter approach direction and ship heading or opening of the hangar door was beneficial to the safe shipboard landing of helicopters. Zhang, Xu and Ball [13] numerically simulated the flow field characteristics of the SFS2 model and obtained calculation results of the velocity field that were in good agreement with the experimental results, indicating the occurrence of a large-scale airflow separation near the hangar. Hodge, Zan and Roper [14] investigated the wake characteristics of the SFS model under unsteady conditions, observing that wake unsteadiness led to increased pilot control loads. Lee and Silva and Meakin [15,16] investigated ship-rotor interactional aerodynamics using overset grids and obtained computational results demonstrating the agreement between CFD-simulated downwash velocity and actual flight test data. Huang, Xu and Shi [17,18] adopted the Reynolds-averaged Navier-Stokes (RANS) method to investigate the flow field characteristics near the ship deck under different hangar door states, revealing that opening the hangar door enhanced the safety of helicopter landings. Zhang, Zhao and Sun [19] numerically simulated an LHA ship using the Fluent software to analyze the flow field structure, helicity and turbulence energy during the simultaneous hover of multiple helicopters under different wind conditions, revealing a detrimental impact of multi-rotor flow field interactions with the stern flow field on helicopter takeoffs and landings. Su, Shi, Xu and Zong [20] numerically simulated helicopter/ship coupling using RANS equations, identifying strong "vortex-vortex" interactions between the rotor, stern and both sides of the deck when a helicopter lands on a ship, resulting in significant oscillations in the rotor thrust. Zong, Zong, Li and Zhao [21] investigated the coupled flow characteristics of a ship model and rotor using the momentum source method and the moving-embedded grid method, finding that the presence of the ship superstructure increased the downwash velocity of the rotor, consequently reducing the rotor thrust. Zhao, Wang and Li [22] reviewed the current research progress on the flow field characteristics of ship surfaces and discussed the critical techniques from three aspects: ship measurement, the wind tunnel test and numerical simulation.

The aforementioned studies mainly focus on the rotor/ship wake interaction under uniform inflow conditions, which differs significantly from that in actual helicopter takeoffs and landings at sea. As a result, these findings may not be applicable for guiding shipboard helicopter maneuvers. Hence, this paper aims to examine the flow field characteristics with rotor/ship wake interaction under atmospheric boundary layer (ABL) conditions, providing a theoretical basis for shipboard helicopter takeoff and landing maneuvers.

## 2. Numerical Simulation Method

### 2.1. Grid Generation

In this paper, the internationally recognized Simplified Frigate Shape (SFS2) model is employed for investigation purposes. Although certain structures, such as radar and gun, have been simplified compared to physical ships, the model still captures the essential flow

field characteristics observed in real frigates. Corresponding wind tunnel tests have been carried out by several research institutions [5,23–25]. The SFS2 model has a total length of 138.68 m, as shown in Figure 1 (in m). The flight deck spans a length of 27.43 m, the hangar features a height of 6.1 m, and the ship has a width of 13.72 m. The model consists of 5.88 million isolated grids, which are 1242 m in length (9 times the ship length), 828 m in width (6 times the ship length) and 120 m in height in total [25], as shown in Figure 2.

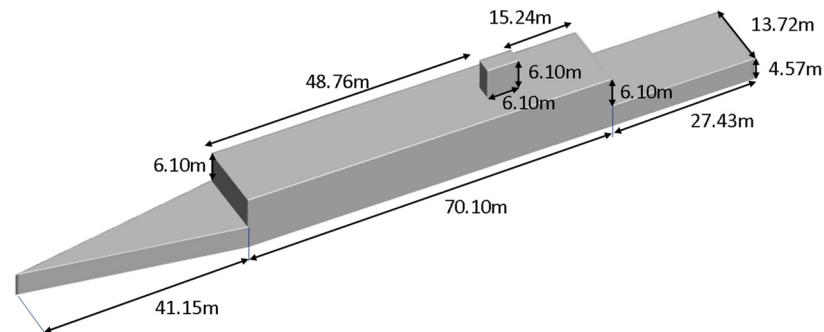


**Figure 1.** Size of SFS2 ship model (in m).

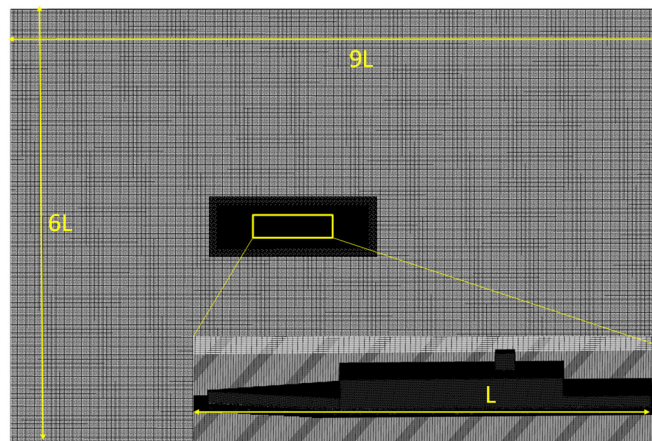


**Figure 2.** Grid of ship model.

With the addition of a rotor, local grid refinement is performed at the rotor position. Following refinement, there are 8 million grids in total, as shown in Figure 3. With rotor/ship coupling, the rotor load is loaded using the momentum source method.

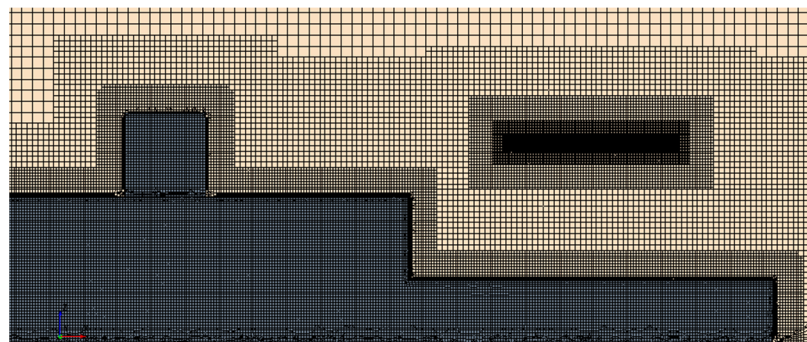


**Figure 3.** Computational grid for rotor/ship coupling.

## 2.2. Turbulence Model

The flow of fluids is usually simulated using the Navier–Stokes (N–S) equations. To ensure an accurate calculation of the vortex structure in the ship's wake zone, this paper

employs the DDES method based on the  $k-\omega$  SST turbulence model for solving the N-S equations. To transition from RANS to Large Eddy Simulation (LES), the dissipative term of the turbulent kinetic energy transport equation of the SST model is rewritten as the ratio of grid scale  $\Delta$  to turbulence length scale  $L_t$  in the implementation of a DDES model, i.e.,  $\beta^* \rho \omega K$  is substituted by:

$$\beta^* \rho \omega K \cdot F_{DES} \tag{1}$$

where,

$$F_{DES} = \max \left[ \frac{L_{SST}}{C_{DES} \Delta}, 1 \right] \tag{2}$$

where,  $L_{SST}$  is the characteristic length for SST in RANS, and  $C_{DES}$  is an adaptive parameter:

$$C_{DES} = (1 - f_1) C_{DES}^{k-\varepsilon} + f_1 C_{DES}^{k-\omega} \tag{3}$$

$$C_{DES}^{k-\varepsilon} = 0.61, \quad C_{DES}^{k-\omega} = 0.78$$

### 2.3. Isolated Ship Example Validation

To validate the accuracy of the numerical simulation, this section examines the flow field characteristics of the SFS2 ship at a wind velocity of 20.58 m/s and a Reynolds number of  $2.26 \times 10^7$ . For the numerical simulation, the SIMPLEC algorithm with a second-order upwind scheme is used, and the unsteady time step is set to 0.0001 s. The velocity inlet and pressure outlet boundary conditions are considered in the simulation, including a non-slip boundary condition for the bottom (sea surface), a free outlet boundary condition for the top and side walls and a non-slip boundary condition for the hull wall surface. Figure 4 illustrates a comparison between the simulated non-dimensional velocity in the rear flow field of the flight deck and the test data [25]. The x-axis in the figure represents the width coordinate of the flight deck (axis position  $y = 0$  m), and the y-axis represents the non-dimensional velocity with reference to the inflow wind velocity (20.58 m/s = 40 kn). The simulated result is the arithmetic average of the data extracted within the final second. The velocity monitoring point is set at the midpoint of the length of the flight deck, aligned in height with the top of the hangar and spanning twice the width of the deck. As shown in the figure, the simulated results agree well with the corresponding test data.

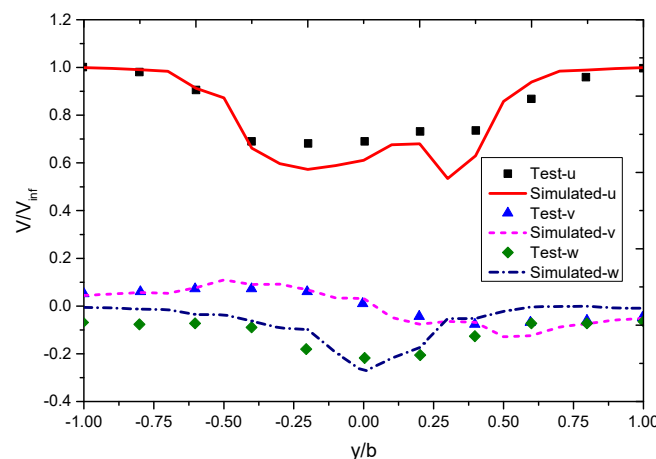


Figure 4. Comparison of simulated velocity with test data.

### 3. Research Analysis

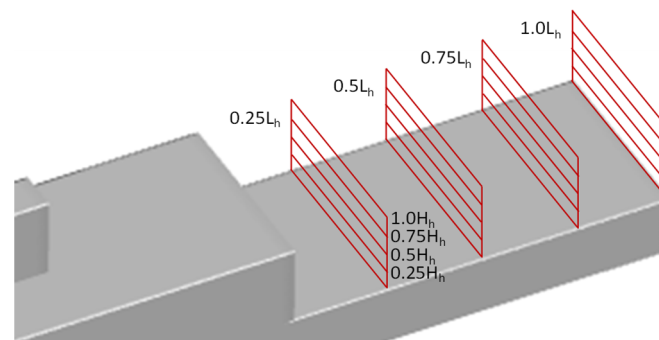
To investigate the wake characteristics of the flight deck when influenced by rotors, this paper calculates the wakes for various simulation scenarios, as given in Table 1. In this investigation, the freestream velocity for the simulation is constant at 20.58 m/s, taking into account that the speed of a warship (30 kn) is usually coupled with wind speed (10 kn).

**Table 1.** Simulation scenarios.

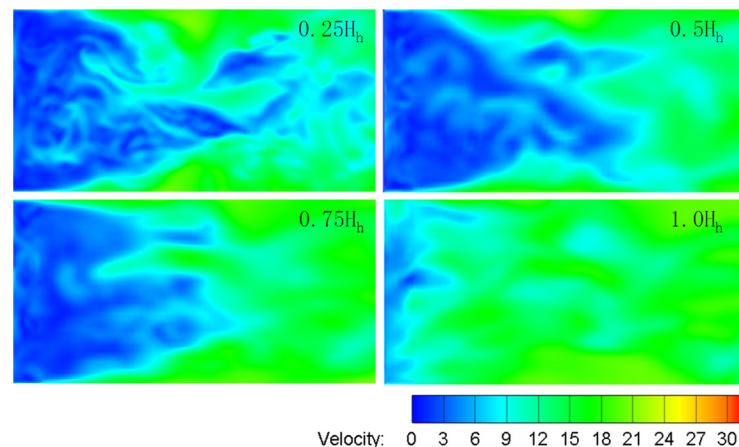
	Ship-Rotor Coupling	Wind Shear
Case 1	×	×
Case 2	✓	×
Case 3	✓	✓

### 3.1. Wake Characteristics of an Isolated Ship under Uniform Inflow Conditions

This section examines the velocity distribution at various stern heights under conditions of uniform inflow and a turbulent intensity of 5% (Case 1). In the stern velocity monitoring section as shown in Figure 5,  $L_h$  represents the length of the flight deck, and  $H_h$  represents the height of the hangar.

**Figure 5.** Distribution of velocity monitoring section.

The velocity distribution characteristics at various locations on the flight deck, as shown in Figure 6, reveal that the velocity deficit primarily occurs near the hangar. As the height increases, the velocity deficit in the wake zone of the flight deck gradually decreases. The velocity deficit at different heights is distributed following a parabolic pattern, primarily because the airflow energy at different velocities around the ship continuously flows into the wake through the velocity shear layer. Moreover, as the height increases, the parabolic shape becomes more flattened, indicating a faster injection of energy and, consequently, a rapid recovery of velocity in the wake zone. The simulation results reveal that the flow field velocity at the flight deck position is not axially symmetric. This asymmetry is mainly caused by the detached eddy generated by the front structure of the flight deck, which enters the deck wake, causing velocity disturbances and obvious irregular pulsations.

**Figure 6.** Velocity distribution at various heights of isolated ship.

Based on the velocity distribution observed at various longitudinal positions of the flight deck as shown in Figure 7, an obvious velocity deficit occurs at the flight deck position

under the influence of the front structure of the flight deck. The magnitude of the velocity deficit increases as the position approaches the leading edge of the flight deck (hangar). In the middle section of the flight deck, the velocity deficit area experiences more significant fluctuations, because the shear flow of the sides of the shipboard would inject the wake vortex and, consequently, the vortex is distorted.

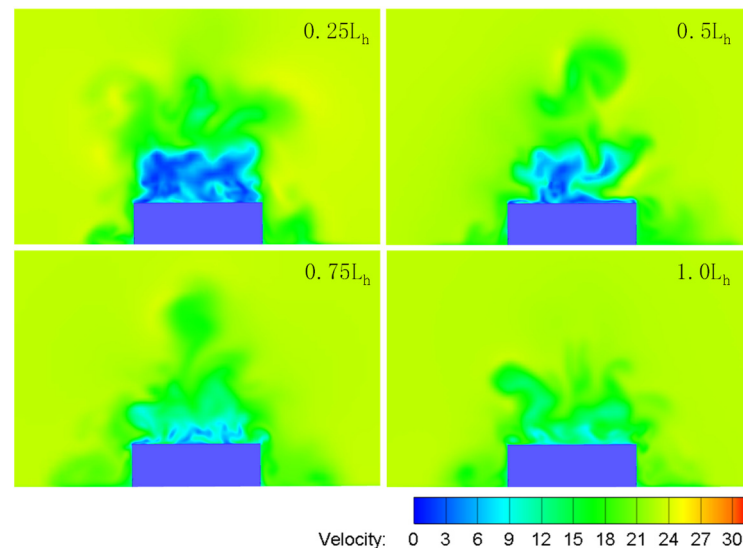


**Figure 7.** Velocity distribution at different deck sections.

The Q-criterion distribution for the flow field of an isolated ship (isosurface set to 5, with velocity dyeing), as shown in Figure 8, reveals that unsteady vortices are primarily concentrated near the bridge and the flight deck. Consequently, shipboard helicopter landings can be influenced by these complex unsteady vortices. The figure also demonstrates that greater vortex field velocities are observed near the bridge, while smaller vortex field velocities are observed near the flight deck. This variation can be attributed to the leeward zone of the front structure, where the flight deck is located. Meanwhile, the chimney can also generate a stronger  $\Omega$ -type separated vortex as the airflow passes over its top.

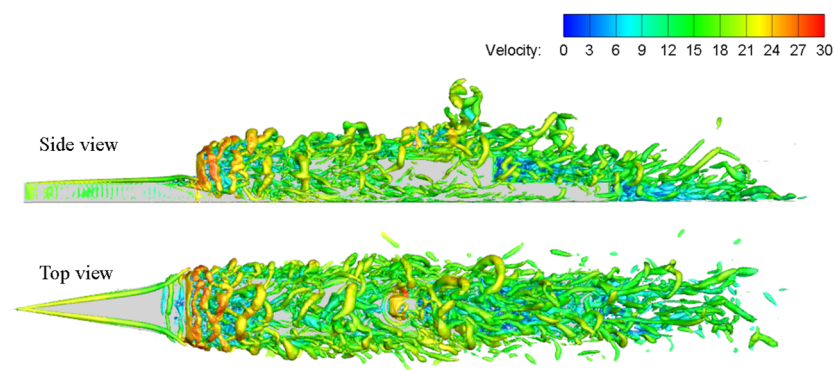


**Figure 8.** Q-criterion distribution on isolated ship.

### 3.2. Flow Field Characteristics with Rotary Interference

To address the influence of rotor downwash flow on the flow field characteristics of the flight deck, this section investigates the flow field characteristics in a rotor/ship coupling scenario (Case 2). The rotor center is positioned at the center of the deck, and the hovering height is 10.0 m above the deck plane. The rotor used in the simulations is a modified version based on the AS-365 N helicopter, and the details of the model rotor are listed in Table 2.

**Table 2.** Rotor parameter.

Rotor Parameter	Value
Rotor diameter	11.93 m
Root cutout	1.4316 m
Airfoil	NACA0012
Chord length	0.385 m
Twist	$-10^\circ$
Blade tip Mach number	0.643
Rotor speed	36.6 rad/s
Pitch angle	$12.82^\circ$
Number of blades	4

The velocity distribution at various heights of the flight deck under uniform inflow conditions (inflow wind velocity 20.58 m/s), as shown in Figure 9, reveals notable differences in the wake distribution between the rotor/ship coupling scenario and an isolated ship scenario. Under the influence of the rotor downwash, the wake velocities exhibit more intricate and significant fluctuations, because the rotor downwash can disrupt the vortex structure of the wake. These velocity fluctuations can be observed even in the immediate vicinity of the hangar. According to the velocity distribution at various deck positions, as shown in Figure 10, the velocity fluctuation increases near the section close to the hangar. A location closer to the stern indicates a large acceleration zone induced by the rotor downwash.

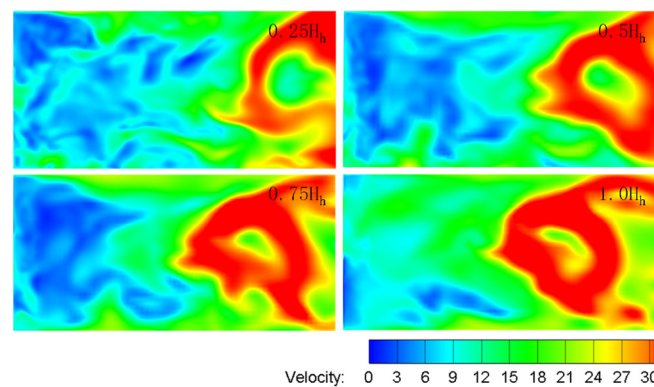
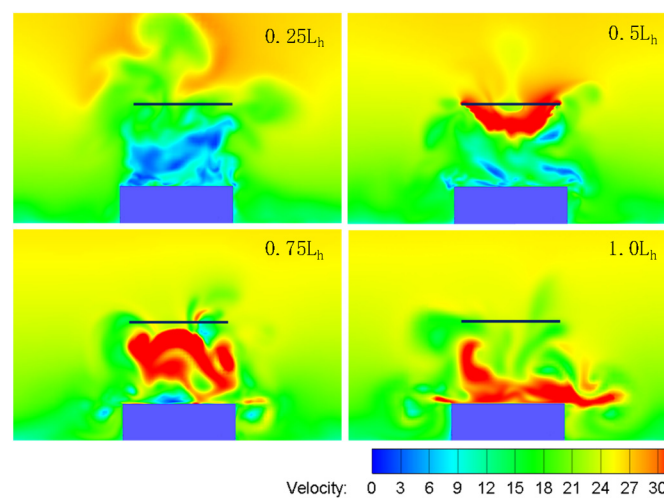
**Figure 9.** Velocity distribution at various heights in a coupling scenario.**Figure 10.** Velocity distribution at various deck sections.

Figure 11 shows the velocity distribution at a point set at the midpoint of the length of the flight deck, aligned with the top of the hangar and spanning twice the width of the ship deck. The figure illustrates the significant downward velocity (component  $w$  of the velocity) perpendicular to the direction of the flight deck under the effect of the rotor downwash. Furthermore, the induced rotor blade tip vortex leads to a W-shaped velocity deficit distribution for the inflow velocity (component  $u$  of the velocity) because the blade tip vortex transport direction is different from the freestream direction.

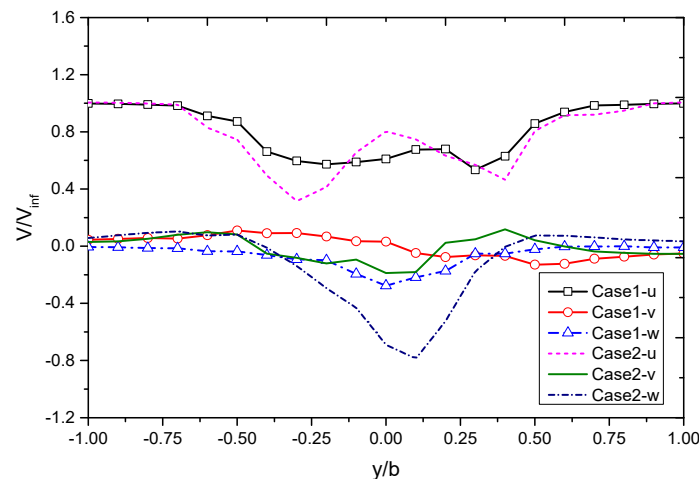


Figure 11. Velocity distribution in a rotor/ship coupling scenario.

According to the  $Q$ -criterion distribution ( $Q = 5$ ) shown in Figure 12, the vortex distribution in the flight deck position is richer than the wake vortex distribution of an isolated ship due to the presence of the rotor wake vortex, which has a longer vortex evolution zone and a  $\lambda$ -shaped distribution, because the weaker strength of the wake vortex relative to the blade tip vortex means it is more susceptible to being sucked into the latter. Additionally, the higher energy (represented by greater velocity) associated with the rotor blade tip and the induction of the tip vortex lead to the absorption of the detached eddy in the wake zone by the blade tip vortex, as shown in Figure 13 ( $Q = 50$ ). Therefore, compared with an isolated ship, the separation vortex is more intense and, consequently, influences a larger zone.

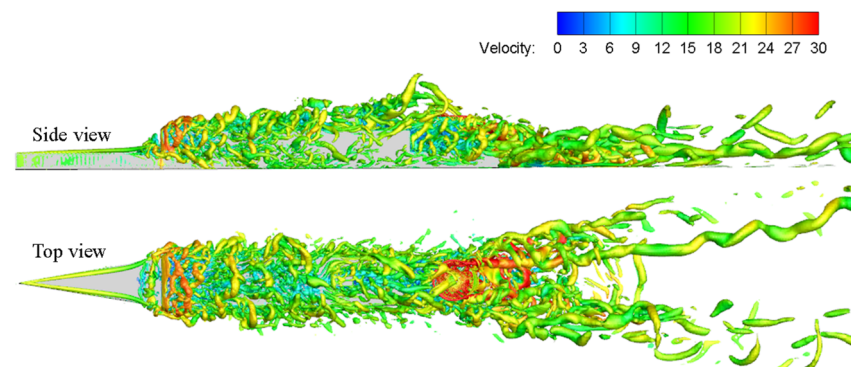
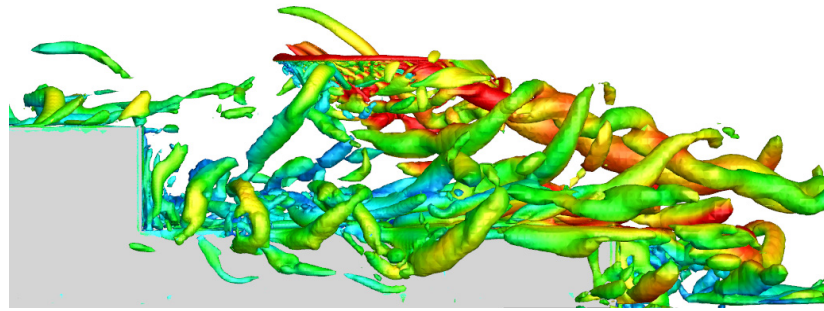


Figure 12.  $Q$ -criterion distribution in a rotor/ship coupling scenario.





**Figure 13.** Q-criterion distribution in the flight deck position.

### 3.3. Characteristics of Rotor/Ship Flow Field under Wind Shear Conditions

This section presents the simulation of flow field under wind shear conditions (Case 3) to investigate the influence of the ship wake on shipboard helicopter landings under real wind conditions. The ABL velocity distribution is modeled using the exponential law, as shown in Figure 14, where the wind profile index is 0.12, the hangar height (i.e., 10.67 m) serves as the reference height and the reference velocity is 20.58 m/s.

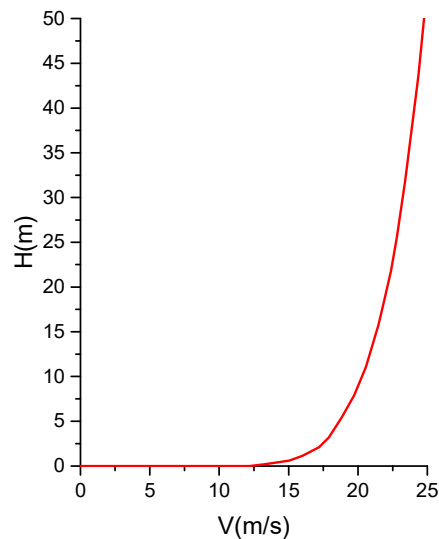


**Figure 14.** Wind profile of atmospheric boundary layer velocity.

The velocity distribution at various deck heights, as shown in Figure 15, reveals that the velocity fluctuates more significantly under shear flow compared to uniform inflow conditions. Additionally, the velocity deficit mainly occurs in the middle of the hangar height and is less pronounced near the flight deck. Comparing this velocity distribution with the downwash velocity distribution under uniform inflow conditions (Figure 9) reveals that wind shear disrupts the ring-shaped distribution structure of the downwash velocity. This disruption primarily arises from the increased velocity mixing effect associated with the inflow shear layer under the wind shear, thereby breaking the tip vortex structure of the rotor downwash. Meanwhile, the cyclic structure of the rotor downwash is also compromised due to the higher wind shear force imparted by the wind shear flow.

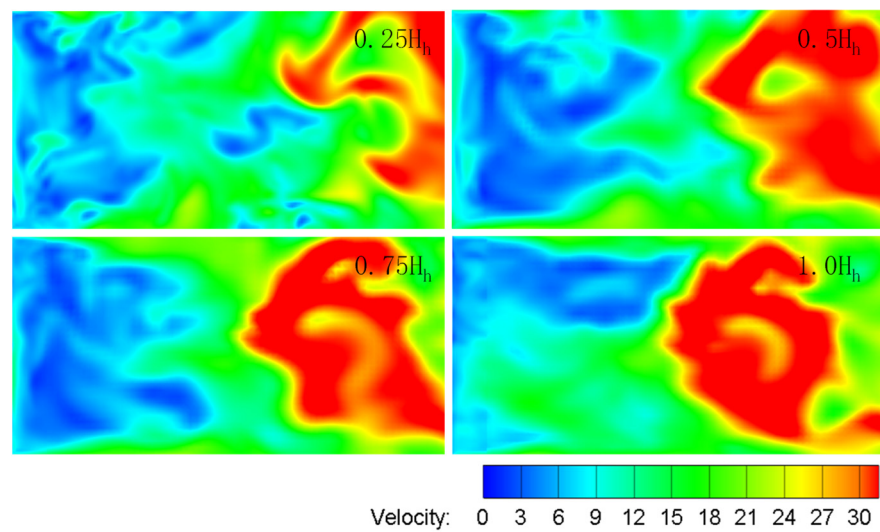


**Figure 15.** Velocity distribution at various heights under wind shear conditions.

The velocity distribution at various deck positions, as shown in Figure 16, reveals that the presence of shear flow amplifies velocity pulsations in the wake deficit zone and leads to a less symmetric rotor downwash compared to uniform inflow conditions. This phenomenon occurs mainly because the turbulent pulsations under shear flow are more likely to enter the wake field, resulting in more pronounced vortex fluctuations.

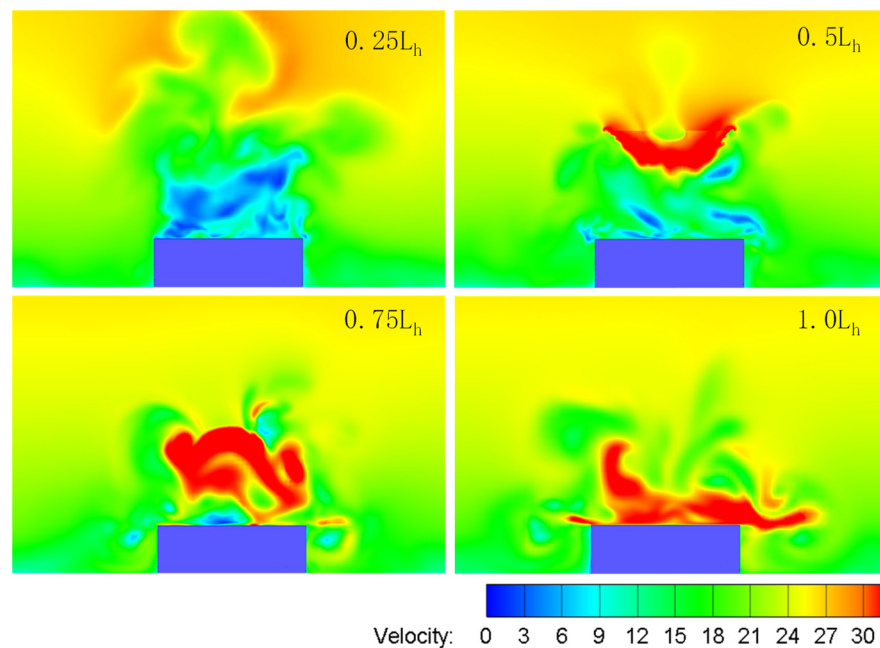


**Figure 16.** Velocity distribution at various deck positions.

The velocity distribution in different directions at the hangar height under wind shear conditions, as shown in Figure 17, reveals minor velocity fluctuations in different directions, with a smaller velocity deficit compared to uniform inflow conditions. The reduced velocity fluctuations in different directions can primarily be attributed to the velocity gradient induced by wind shear, which facilitates more rapid energy exchange between different height positions and aids in velocity recovery.

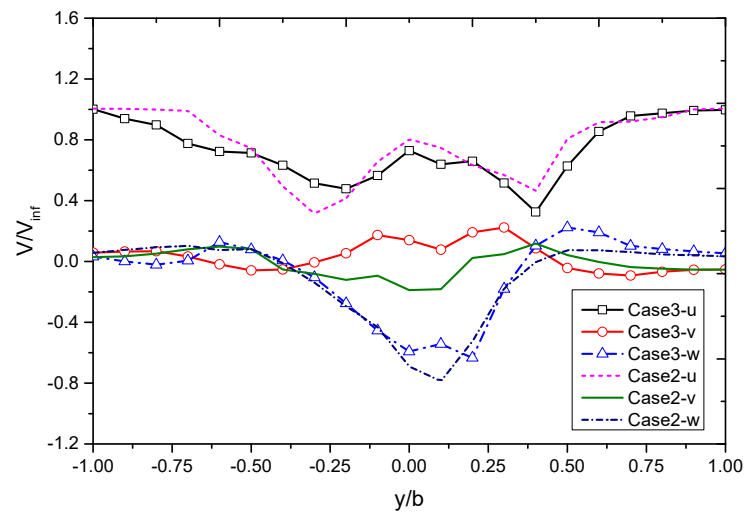


**Figure 17.** Velocity distribution under wind shear conditions.

The Q-criterion distribution ( $Q = 5$ ) shown in Figure 18 reveals that the induction of the tip vortex results in the absorption of turbulent vortex in the wake zone by the tip vortex, reducing the occurrence of detached eddies behind the deck axis. When comparing the wake characteristics of Case 2 and Case 3, we find that the detached eddy behind the hangar under wind shear conditions is considerably weaker compared to uniform inflow conditions, as indicated by the black circle in Figure 19 ( $Q = 50$ ). This reduced detached eddy is possibly attributed to the additional viscosity generated by wind shear, which leads to the quick decay of the eddy.

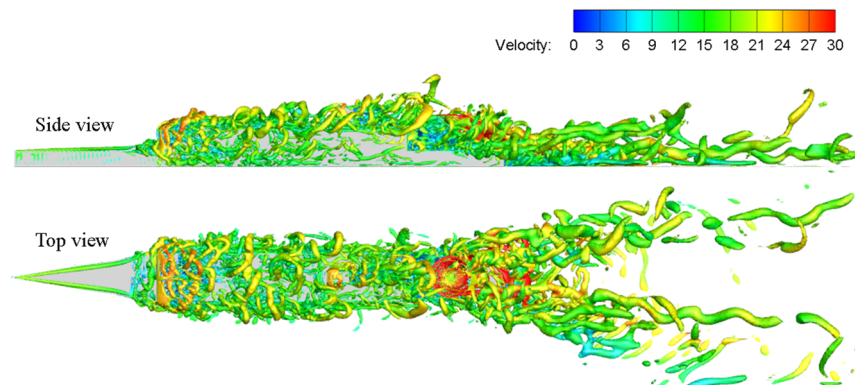


**Figure 18.** Q-criterion distribution in rotor/ship coupling scenario.

In Figure 20, we compare the turbulence viscosity distribution at various heights under uniform inflow and wind shear conditions. The turbulence viscosity distribution under wind shear conditions exhibits some changes relative to uniform inflow conditions. Specifically, the turbulence viscosity decreases near the flight deck position and increases at the hangar height. The presence of wind shear diminishes the wind velocity near the flight deck position, thereby leading to a relatively smaller energy injection into the wake compared to uniform inflow conditions. As the height increases, the wind velocity rises, resulting in increased energy injection into the wake under the influence of the shear layer.

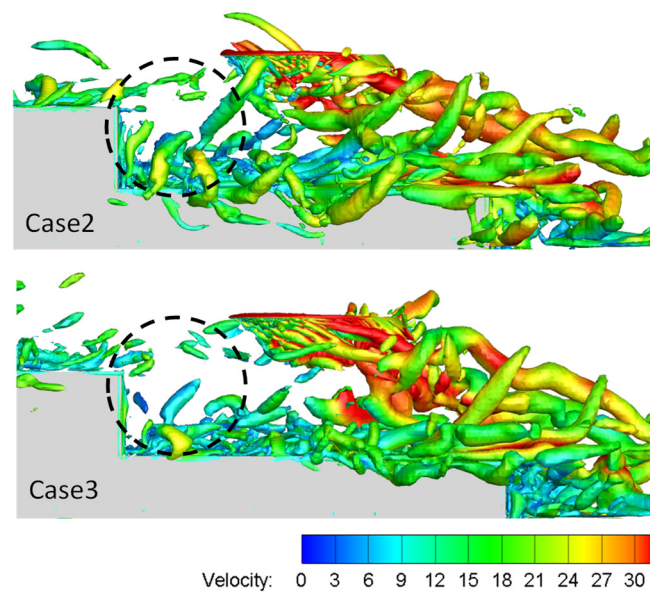


Figure 19. Q-criterion distribution near flight deck.

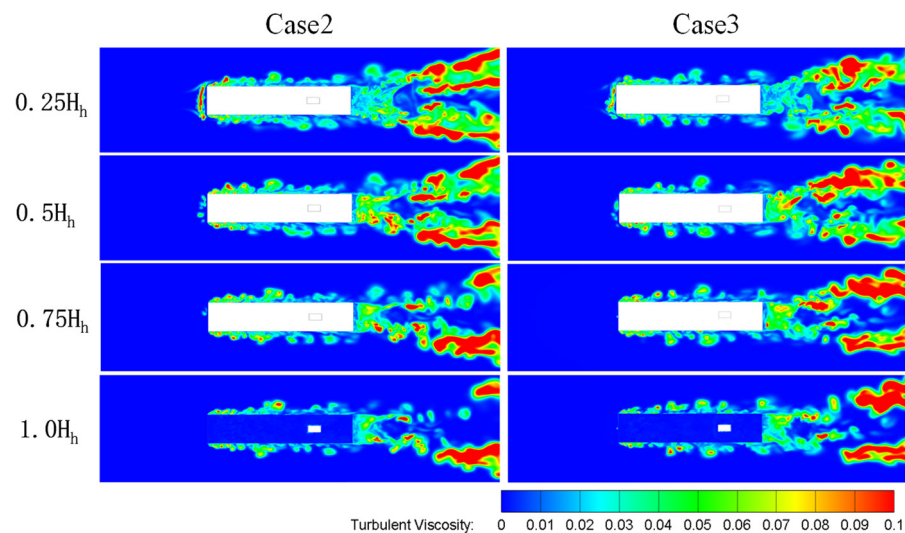


Figure 20. Turbulence viscosity distribution at various heights.

#### 4. Conclusions

This paper numerically simulates the wake characteristics in the context of helicopter rotor/ship interaction. The following conclusions are drawn through a comparative analysis of the isolated ship scenario under uniform inflow conditions, the rotor/ship coupling scenario under uniform inflow conditions and the rotor/ship coupling scenario under wind shear conditions:

- (1) Under uniform inflow conditions, the velocity deficit at various heights on the flight deck of an isolated ship is distributed following a parabolic pattern, with the parabolic shape becoming more flattened as the height increases.
- (2) In the rotor/ship coupling scenario, the inflow velocity in the wake zone is distributed in a “W” shape due to the influence of the rotor blade tip vortex.
- (3) Under wind shear conditions, the influence of the rotor on the wake is diminished, resulting in minor velocity fluctuations compared to uniform inflow conditions, and the detached eddy is suppressed to some extent.

**Author Contributions:** Conceptualization, G.L. and Q.W.; methodology, Q.Z.; software, G.Z.; validation, G.L., Q.W. and G.Z.; resources, L.W.; data curation, F.F.; writing—original draft preparation, G.L.; writing—review and editing, Q.W.; project administration, G.L.; funding acquisition, G.L. All authors have read and agreed to the published version of the manuscript.

**Funding:** This work was supported by the Pre research project, China aerodynamics research and development center (50906030601); Exploratory research project, China aerodynamics research and development center (JK20211A020092); Open research project of key laboratory of rotor aerodynamics, China aerodynamics research and development center (RAL202201).

**Conflicts of Interest:** The authors declare no conflict of interest.

## References

1. Crozon, C.; Steijl, R.; Barakos, G.N. Numerical Study of Helicopter Rotors in a Ship Airwake. *J. Aircr.* **2014**, *51*, 1813–1832. [[CrossRef](#)]
2. Gu, Y.; Ming, X. Experimental investigation on flow field properties around aft-deck of destroyer. *Acta Aeronaut. Astronaut. Sin.* **2001**, *22*, 500–504. (In Chinese)
3. Polsky, S.A.; Bruner, C.W.S. Time-Accurate Computational Simulations of an LHA Ship Airwake. In Proceedings of the 18th Applied Aerodynamics Conference, Denver, CO, USA, 14–17 August 2000.
4. Polsky, S.A. A Computational Study of Unsteady Ship Airwake. In Proceedings of the 40th AIAA Aerospace Sciences Meeting & Exhibit, Reno, NV, USA, 14–17 January 2002.
5. Bunnell, J.B. An Integrated Time-varying Airwake in A UH-60 Black Hawk Shipboard Landing Simulation. In Proceedings of the AIAA Modeling and Simulation Technologies Conference and Exhibit, Montreal, QC, Canada, 6–9 August 2001.
6. Reddy, K.R.; Toffoletto, R.; Jones, K.R.W. Numerical simulation of ship airwake. *Comput. Fluids* **2000**, *29*, 451–465. [[CrossRef](#)]
7. Rajagopalan, R.G.; Schaller, D.; Wadcock, A.; Yamauchi, G.; Heineck, J.; Silva, M. Experimental and Computational Simulation of a Model Ship in a Wind Tunnel. In Proceedings of the 43rd AIAA Aerospace Sciences Meeting and Exhibit, Reno, NV, USA, 10–13 January 2005.
8. Brooks, J.M.; Gupta, A.K.; Smith, M.; Marineau, E.; Tatum, K.E. High-Speed Local Particle Injection for Particle Image Velocimetry. *AIAA J.* **2019**, *57*, 4490–4503. [[CrossRef](#)]
9. Liu, H.; Feng, Y.; Zheng, X. Experimental investigation of the effects of particle near-wall motions on turbulence statistics in particle-laden flows. *J. Fluid Mech.* **2022**, *943*, A8. [[CrossRef](#)]
10. Sezeruzol, N.; Sharma, A.; Long, L.N. Computational fluid dynamics simulations of ship airwake. *Proc. Inst. Mech. Eng. Part G J. Aerosp. Eng.* **2005**, *219*, 369–392. [[CrossRef](#)]
11. Zhao, W. Research on Test Approach to Complex Wake Between the Helicopter Rotor Induced Flow and the Warship Airwake. *Flight Dyn.* **2007**, *25*, 72–74. (In Chinese)
12. Zhao, W. PIV measurements of the warship airwake. *J. Exp. Fluid Mech.* **2007**, *21*, 32–35. (In Chinese)
13. Zhang, F.; Xu, H.; Ball, N.G. Numerical Simulation of Unsteady Flow over SFS 2 Ship Model. In Proceedings of the 47th AIAA Aerospace Sciences Meeting Including the New Horizons Forum and Aerospace Exposition, Orlando, FL, USA, 5–8 January 2009.
14. Hodge, S.J.; Zan, S.J.; Roper, D.M.; Padfield, G.D.; Owen, I. Time-Accurate Ship Airwake and Unsteady Aerodynamic Loads Modeling for Maritime Helicopter Simulation. *J. Am. Helicopter Soc.* **2009**, *54*, 022005. [[CrossRef](#)]
15. Lee, Y.; Silva, M. CFD modeling of rotor flowfield aboard ship. In Proceedings of the 48th AIAA Aerospace Sciences Meeting Including the New Horizons Forum and Aerospace Exposition, Orlando, FL, USA, 4–7 January 2010.
16. Meakin, R.L. A new method for establishing intergrid communication among systems of overset grids. In Proceedings of the 10th Computational Fluid Dynamics Conference, Honolulu, HI, USA, 24–27 June 1991.
17. Huang, B.; Xu, G.; Shi, Y. Research on Influence of Hangar Door Opening and Closing on Landing Flow-field for Shipborne Helicopters. *J. Nanjing Univ. Aeronaut. Astronaut.* **2015**, *47*, 198–204. (In Chinese)
18. Chen, H.; Xu, G.; Shi, Y. Coupled flow field numerical simulation study of shipborne tilt-rotor aircraft landing area. *Flight Dyn.* **2020**, *38*, 21–26. (In Chinese)
19. Zhang, S.; Zhao, J.; Sun, P. Numerical study of influence of multiple helicopter rotors on warship deck flow field. *J. Dalian Univ. Technol.* **2015**, *55*, 457–463. (In Chinese)
20. Su, D.; Shi, Y.; Xu, G. Numerical simulation of coupled flow field of helicopter/ship. *Acta Aeronaut. Astronaut. Sin.* **2017**, *38*, 80–91. (In Chinese)
21. Zong, K.; Zong, W.; Li, H.; Zhao, P. Research of simulation methods on landing flow field for shipborne helicopters. *Ship Sci. Technol.* **2018**, *40*, 124–130. (In Chinese)
22. Zhao, R.; Wang, C.; Li, H. Progress in ship airwake qualification program. *J. Ship Mech.* **2018**, *22*, 1431–1444. (In Chinese)
23. Snyder, M.R.; Burks, J.S.; Brownell, C.J.; Luznik, L.; Miklosovic, D.S.; Golden, J.H.; Hartsog, M.E.; Lemaster, G.E.; Roberson, F.D.; Shishkoff, J.P.; et al. Determination of shipborne helicopter launch and recovery limitations using computational fluid dynamics. In Proceedings of the 66th American Helicopter Society Annual Forum, Phoenix, AZ, USA, 11–13 May 2010.

24. Syms, G.F. Simulation of simplified-frigate airwakes using a lattice-Boltzmann method. *J. Wind Eng. Ind. Aerodyn.* **2008**, *96*, 1197–1206. [[CrossRef](#)]
25. Forrest, J.S.; Owen, I. An investigation of ship airwakes using detached-edge simulation. *Comput. Fluids* **2010**, *39*, 656–673. [[CrossRef](#)]

**Disclaimer/Publisher’s Note:** The statements, opinions and data contained in all publications are solely those of the individual author(s) and contributor(s) and not of MDPI and/or the editor(s). MDPI and/or the editor(s) disclaim responsibility for any injury to people or property resulting from any ideas, methods, instructions or products referred to in the content.